Available online at www.sciencedirect.com

ScienceDirect

Ceramics International 40 (2014) 2943–2951

CERAMICS INTERNATIONAL

www.elsevier.com/locate/ceramint

Photoinduced electron transfer mechanism between green fluorescent protein molecules and metal oxide nanoparticles

Sabriye Acikgoz[a,d,*], Yakup Ulusu[b], Seckin Akin[c], Savas Sonmezoglu[d], Isa Gokce[e], Mehmet Naci Inci[a]

[a]Department of Physics, Boğaziçi University, Bebek, 34342 Istanbul, Turkey
[b]Department of Bioengineering, Faculty of Engineering, Karamanoğlu Mehmetbey University, Karaman 70100, Turkey
[c]Department of Physics, Faculty of Kamil Özdağ Science, Karamanoğlu Mehmetbey University, Karaman 70100, Turkey
[d]Department of Material Science and Engineering, Faculty of Engineering, Karamanoğlu Mehmetbey University, Karaman 70100, Turkey
[e]Department of Bioengineering, Faculty of Engineering, Gaziosmanpaşa University, Tokat 60240, Turkey

Received 4 September 2013; received in revised form 4 October 2013; accepted 4 October 2013
Available online 16 October 2013

Abstract

Green fluorescent protein (GFP) molecules are attached to titanium dioxide and cadmium oxide nanoparticles via sol–gel method and fluorescence dynamics of such a protein–metal oxide assembly is investigated with a conventional time correlated single photon counting technique. As compared to free fluorescent protein molecules, time-resolved experiments show that the fluorescence lifetime of GFP molecules bound to these metal oxide nanoparticles gets shortened dramatically. Such a decrease in the lifetime is measured to be 22 and 43 percent for cadmium oxide and titanium dioxide respectively, which is due to photoinduced electron transfer mechanism caused by the interaction of GFP molecules (donor) and metal oxide nanoparticles (acceptor). Our results yield electron transfer rates of $3.139 \times 10^8\ s^{-1}$ and $1.182 \times 10^8\ s^{-1}$ from the GFP molecules to titanium dioxide and cadmium oxide nanoparticles, respectively. The electron transfer rates show a marked decrease with increasing driving force energy. This effect represents a clear example of the Marcus inverted region electron transfer process.

Keywords: D. TiO_2; CdO; GFP; Electron transfer

1. Introduction

Green fluorescent protein (GFP) is a protein of 238 amino acids with a molecular weight of 27 kDa, which emits a bright green fluorescence with a peak wavelength at 509 nm when exposed to ultraviolet or blue light. GFP emits green fluorescence without a need in any enzyme or co-factors. The emission of the GFP of the jellyfish *Aequora Victoria* originates from the spontaneous formation of an emitting chromophore inside a rigid β-barrel structure [1]. The GFP fluorescence activity can be detected with minimal handling efforts, for example, it does not need the detection tools like use of a fluorescence microscope, a fluorometer, a fluorescence-activated cell sorting machine, an imaging micro plate reader, or a lysate preparation [2]. Many GFP mutants have been reported in the scientific literature and more than 20 crystal structures of GFP mutants and homologs are listed in the Protein Data Bank [3]. Although the GFP mutants have quite different spectroscopic characteristics, their structural features are remarkably similar [4].

GFP is an accomplished fluorescent molecule widely used in cell imaging applications, gene expression, visualizing protein–protein interactions and protein localization due to its unique characteristics [5–7]. Recently, Bogdanov et al. discovered a new feature of GFPs of diverse origins to act as the light-induced electron donors in photochemical reactions with various electron acceptors [8]. Moreover, the interaction mechanism between fluorescent proteins and nanoparticles

*Corresponding author at: Department of Material Science and Engineering, Faculty of Engineering, Karamanoğlu Mehmetbey University, Karaman 70100, Turkey. Tel.: +90 54 4218 7584; fax: +90 33 8226 2214.
E-mail addresses: sabriyeacikgoz@kmu.edu.tr, sabriyeacikgoz@gmail.com (S. Acikgoz).

0272-8842/$ - see front matter © 2013 Elsevier Ltd and Techna Group S.r.l. All rights reserved.
http://dx.doi.org/10.1016/j.ceramint.2013.10.017

could provide further control over the fabrication of nano-optic and nano-electronic devices. Quenching of green fluorescent molecules, when it is in close proximity to a metal nanoparticle, like gold or silver, has been successfully studied both theoretically and experimentally [9,10]. However, excitation mechanism of GFP-metal oxide nanoparticles (MON) has not been clarified yet, which is envisaged to be one of the most popular parts of the nano-technological applications.

Metal oxide nanoparticles are emerging as highly attractive materials for many fields of technology including catalysis, sensing, optoelectronic devices, environmental remediation and energy conversion [11–13]. The most commonly used metal oxide nanoparticles are titanium dioxide (TiO_2), zinc oxide (ZnO), iron (III) oxide (Fe_2O_3), Chromium (III) oxide (Cr_2O_3) and Cadmium oxide (CdO). Especially, TiO_2 and ZnO are the preferred nanoparticle types due to their large band gap energy and their high electron mobility [14,15]. Stable metal oxide nanoparticles cannot absorb visible light due to their relatively wide band gaps. Sensitization of these metal oxide materials with photo sensitizers – such as with organic dyes – allow absorption of the visible light. Therefore, such systems have been extensively studied in silver halide photography, electrophotography, and – more recently – in solar energy cells [16]. In the sensitization process, the excited dye molecule injects an electron into the conducting band of the metal oxide nanoparticle within a few picoseconds [17]. Then, the oxidized dye is reduced back to its ground state and the injected electron flows through the semiconductor network.

In this paper, the effects of titanium dioxide and cadmium oxide nanoparticles on the fluorescence intensity and lifetime dynamics of the green fluorescent protein molecules are examined. Recently, it has been demonstrated that the band gap energy of a metal oxide nanoparticle is strongly effective on the performance of MON based devices [18]. Therefore, two different metal oxide nanoparticles are studied in this work, one of them with a wide band gap energy (TiO_2, 3.42 eV) and the other with a relatively narrower band gap energy (CdO, 2.36 eV). It is observed that the average lifetime of the GFP molecules on the metal oxide nanoparticles is significantly shortened than that on a glass substrate. As a consequence of photoinduced electron transfer process between GFP and metal oxide nanoparticles, the fluorescence lifetime of GFP on CdO and TiO_2 nanoparticles drops from 2.419 ns down to 1.881 ns and 1.375 ns, respectively. Moreover, the electron injection yield of the GFP/TiO_2 nanoparticle system is expectedly around three times of that of the GFP/CdO nanoparticle system.

Relentless efforts are underway all over the world to obtain efficient photovoltaic energy conversion using dye sensitized metal oxide or semiconductor nanomaterials. During the last few years, a number of dyes, such as phthalocyanines, triphenyl methane, xanthenes, coumarins, porphyrins and ruthenium have been tested as sensitizer [19]. These dyes and those chemically engineered are hard to put up and are too expensive. Therefore, natural dye sensitizers should be investigated to develop low cost and environmental friendly green solar cells. In the present article, photoinduced electron transfer dynamics of GFP bound to TiO_2 and CdO nanoparticles is discussed in details. Our time resolved experimental results suggest that the green fluorescent protein molecules have a great potential to be remarkable candidates as sensitizers in photovoltaic energy conversion devices.

2. Experimental section

2.1. Expression and purification of hexa histidine tagged GFP

The plasmid vector pBAD–GFPuv carrying deoxyribonucleic acid (DNA) fragment encoding for GFP is digested using two different restriction enzymes (*Nhe* I and *Eco* RI) The GFP-encoded DNA fragment is introduced into pET28a plasmid (Merck; Novagen) using *Nhe* I and *Eco* RI restriction sites. The GFP gene is ligated into pET28a after gel purification of both vector and insert. The final plasmid is named pETGFP and DNA sequencing of this plasmid showed that the hexa histidine-tagged GFP-encoded DNA fragment is correctly inserted. Six histidine-tagged GFP is expressed in an *Escherichia coli* BL21 DE3 (pLysE) strain. The strain is transformed with pETGFP plasmid and grown on Luira Bertoni (LB) plates with kanamycin (40 mg/ml) and chloramphenicol (35 mg/ml) selection. Four milliliters of LB medium in a screw capped test tube with antibiotics is inoculated with a single *E. coli* colony and grown overnight at 37 °C. A 4 ml overnight culture is introduced into 600 mL of the LB medium in 2 L flasks containing kanamycin and chloramphenicol. Bacteria are grown up to an optical density (OD 600) of 0.8 and induced by the addition of a final concentration of 1 mM isopropyl-thiogalactopyranoside (IPTG) and then grown for additional 4 h. *E. coli* cells are harvested and resuspended in 20 mM phosphate and 300 mM sodium chloride (NaCl) (pH 8) buffer containing RNAse, DNAse, and protease inhibitors (1 mM phenylmethylsulfonyl fluoride and 1 mM benzamidine). The cells are lysed in a French press and the supernatant is obtained by ultracentrifugation (Beckman Coulter Optima L-80 ultracentrifuge and Ti 45 rotor) at 40,000 rpm (125,000*g*) for 1 h. The N-terminal hexa-histidine-tag facilitated purification of the GFP by means of a Ni–NTA agarose affinity resin (Qiagen). The fusion protein is washed onto the column with a 20 mM phosphate and 300 mM NaCl buffer, and then additionally washed with the same buffer containing 50 mM imidazole and eluted in 300 mM imidazole, pH 7.0. The expression of GFP protein is qualitatively analyzed by sodium dodecyl sulfate polyacrylamide gel electrophoresis (SDS-PAGE) (Fig. 1). The concentration of protein is determined by UV absorption at 280 nm. The molecular weight of the his-tagged GFP is 28.890 kDa and its extinction coefficient is 22.015 M^{-1} cm^{-1} at 280 nm.

2.2. Synthesis of TiO_2 nanoparticle solution

In order to prepare a TiO_2 solution, firstly titanium tetraispropoxide (2.4 mL, $Ti(OC_3H_7)_4$, ex. Ti ≥ 98%, Merck) is added in ethanol (25 mL, C_2H_6O, 99.9%, Merck), and the solution is kept in a magnetic stirrer for one hour. Next, glacial acetic acid (5 mL, $C_2H_4O_2$, 99.9%, Merck), triethylamine (1.5 mL, $(C_2H_5)_3N$, 99%, Merck) and ethanol (25 mL) are added to the solution. After, it is mixed in the magnetic stirrer

for 1 h. Also, to obtain the GFP-doped TiO_2 solution, GFP is added into the undoped TiO_2 solution, and the solution is subjected to the magnetic stirrer for two additional hours. Finally, the pure and GFP-doped TiO_2 solution is aged at room temperature for one day before deposition.

2.3. Synthesis of CdO nanoparticle solution

In order to prepare a CdO solution, first, 1 mol cadmium acetate [$Cd(CH_3COO)_2+2H_2O$, Merck] is added in 46 mol methanol solvent [CH_3OH, Merck] and the solution is kept in a magnetic stirrer for 1 h. Then, 0.2 mol glycerol [$C_3H_8O_3$, Merck] and 0.5 mol triethylamine [$C_8H_{15}N$, Merck] are added in the solution, and after, it is mixed in the magnetic stirrer for 1 h. To obtain the GFP-doped CdO solution, GFP is added into the undoped CdO solution, and the solution is subjected to the magnetic stirrer for two additional hours. Finally, the pure and GFP-doped CdO solution is aged at room temperature for one day before deposition.

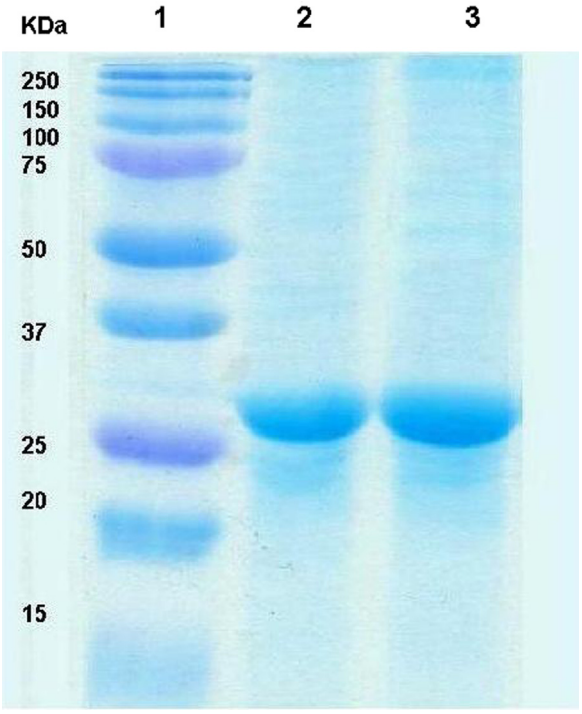

Fig. 1. A photograph of 12% SDS-PAGE of expressed GFP protein. Lane 1 molecular weight marker (BIO-RAD Dual Color Precision Plus Protein standard), lanes 2 and 3, elution of His-tagged GFP with 300 mM imidazole.

2.4. Fabrication of thin films

Microscope glass slides are used as the substrates for thin films. Prior to deposition, the glass slides are sequentially cleaned in an ultrasonic bath with acetone and ethanol. Finally they are rinsed with distilled water and dried. After the above treatment, spin coating process is applied to cover solutions on the glass substrates. The spinning process is performed using Holmarc Spin Coating Unit and coating is done by rapidly depositing 0.6 mL of solution onto a glass substrate spun at 6000 rpm for 30 s in air. In order to obtain as-deposited films, ten spin coated layers are carried out on each substrate.

2.5. Time-resolved lifetime and fluorescence intensity Measurements

Time resolved fluorescence lifetime and fluorescence intensity measurements are performed using a TimeHarp 200 PC-Board system (Picoquant, GmbH) and a fiber optic spectrometer (USB-VIS–NIR Ocean Optics), respectively [20]. Fig. 2 shows the optical experimental setup. The excitation source used in the experiment is an ultraviolet pulsed diode laser head with a wavelength of 405 nm (LDH-C-D-470 Picoquant, GmbH). According to the GFP absorbance (excitation) spectrum, which is given in Fig. 4, GFP has two excitation peaks. The major excitation peak is observed at 395 nm and a minor peak at 475 nm. Therefore, the near UV light is an excellent excitation source, as GFP's chromophore absorbs at a wavelength of 395 nm, exciting the electrons in the chromophore and boosting them to a higher energy state. In order to obtain a

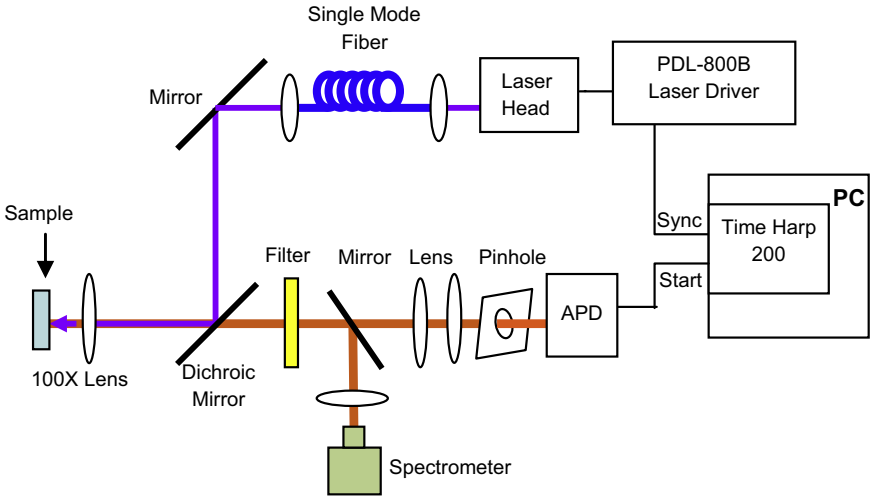

Fig. 2. Optical setup.

Gaussian beam illumination, a single mode optical fiber is used as a waveguide (Thorlabs, S405-HP). The separation of the fluorescence emission and the excitation occurs at a dichroic mirror. The excitation light is focused onto the sample using a microscope objective of 0.55 numerical apertures with a working distance of 10.1 mm (Nikon, ELWD 100 ×). A confocal pinhole, which has a diameter 75 μm, is placed in the focal plane, to exclude out of focus background fluorescence. The optical system used in our experimental work is based on a confocal light detection scheme via a 75 μm pinhole in the setup, which allows monitoring the reflected light coming from the very center of the small focused area only. In other words, the possibility of getting illuminations apart from the focal center is eliminated by this pinhole.

For multi-exponential fluorescence decay fitting, FluoFit computer program (Picoquant, GmbH) is used. The fluorescence intensity decays is recovered from the frequency-domain data in terms of a multiexponential model

$$I(t) = \sum_{i=1}^{n} A_i \exp(-t/\tau_i) \quad (1)$$

where A_i is the amplitude of each component and τ_i is its lifetime. The fractional contribution of each component to the steady-state intensity is described by

$$f_i = \frac{A_i \tau_i}{\sum_j A_j \tau_j} \quad (2)$$

the intensity weighted average lifetime is represented as

$$\langle \tau \rangle = \sum_i f_i \tau_i \quad (3)$$

and the amplitude-weighted lifetime is given by

$$\overline{\tau} = \frac{\sum_i A_i \tau_i}{\sum_i A_i} \quad (4)$$

3. Results and discussion

The size measurements of metal oxide nanoparticles are accomplished by means of a scanning electron microscope (SEM). Fig. 3 shows SEM micrographs of top view of the GFP fluorescent protein coated CdO and TiO_2 nanoparticles. The mean diameter of CdO and TiO_2 nanoparticles are measured as 34.53 ± 4.82 nm and 31.25 ± 3.25 nm, respectively. Especially, in solar cell structures, two electrically conducting phases must inter-penetrate completely to allow full closed circuit operation. According to the SEM images, our nanoparticles are well connected to their neighbors and they satisfy this condition.

The UV–vis. absorption spectra of the metal oxide nanoparticles and green fluorescent protein are obtained to determine the relationship between the band gap energy values and the electron transfer efficiency. The fundamental absorption spectra, which correspond to electron excitation from the valence band to conduction band, are recorded with a Shimadzu 3600 UV–vis–NIR spectrometer, as shown in Fig. 4. The optical band gap energies of metal oxide nanoparticles are calculated using Tauc relation [21]. The calculated values of direct optical band gap are 3.42 and 2.36 eV for TiO_2 and CdO nanoparticles, respectively. The shift from $E_{gap}=3.2$ eV for bulk anatase TiO_2 to $E_{gap}=3.42$ eV for nanoparticles is interpreted as a result of a quantum size effect. It is observed that addition of GFP on the metal oxide nanoparticle surface shifts the onset of absorption to the visible range and GFP molecules leads to a decrease in the band gap energy values of metal oxides. Calculated band gap values are 3.37 and 2.26 eV for GFP doped TiO_2 and CdO nanoparticles, respectively. This result is clear evidence that GFP fluorescent molecules are chemically bonded to the metal oxide nanoparticles. In addition, the decrease in the band gap energy values of the GFP doped nanoparticles, probably due to adhesion of the nanoparticles. Energy difference between the first excited state and the ground state of GFP is calculated as 2.25 eV.

Metal oxide nanoparticles shown in Fig. 3 are impregnated by GFP fluorescent protein molecules and the fluorescence intensity and spontaneous emission rate of GFP are studied in the optical setup shown in Fig. 2. It is observed that the free GFP, which is coated on a microscope slide, exhibits a bright emission spectrum with a peak wavelength at about 509 nm under the illumination of 405 nm pulsed diode laser. GFP dye molecules are chemically attached to TiO_2 and CdO metal oxide nanoparticles. Although concentration of GFP fluorescent protein is kept constant for all samples, a significant reduction in the fluorescence intensity of GFP is observed (see Fig. 5). This result indicates that the metal oxide nanoparticles quench the fluorescence of GFP molecules. Moreover, our steady state fluorescence studies show that the effect of TiO_2 nanoparticles on the fluorescence intensity of GFP is more effective than CdO nanoparticles. The fluorescence quenching of GFP molecules on the metal oxide nanoparticles is ascribed to the environmental change to the GFP core chromophore which is highly protected by the beta sheet barrel structure. Fluorescence is not an inherent property of the isolated fluorophore, the elucidation of its three-dimensional structure will help provide an explanation for the generation of fluorescence in the mature protein. Spectral properties of a common fluorophore are altered as a function of protein environment within red, blue, or green opsins. In our samples, the characteristic of fluorescence spectrum of our GFP remains the same, therefore; it is obvious that the barrel structure does not change when attached to the metal oxide nanoparticles.

The time-resolved fluorescence lifetime of the GFP molecule is performed using the PCI-Board system (TimeHarp 200, PicoQuant). The measurement of the fluorescence lifetime is based on the time correlated single photon counting (TCSPC) method. In this method, the time between the detected single photon of the fluorescence (start signal) and the excitation laser pulse (stop signal) is measured. The measured data is plotted as a fluorescence lifetime histogram. Decay parameters are determined using the double exponential tailfit model, and the best fits are obtained by minimizing χ^2 values as seen in Fig. 6.

The spontaneous emission of an emitter is not an intrinsic property of the emitter and it is strongly affected by the surrounding environment. Therefore, the decay lifetime of an emitter in the vicinity of a nano-structure is inhibited or enhanced. Such structure may be, for example, a flat surface,

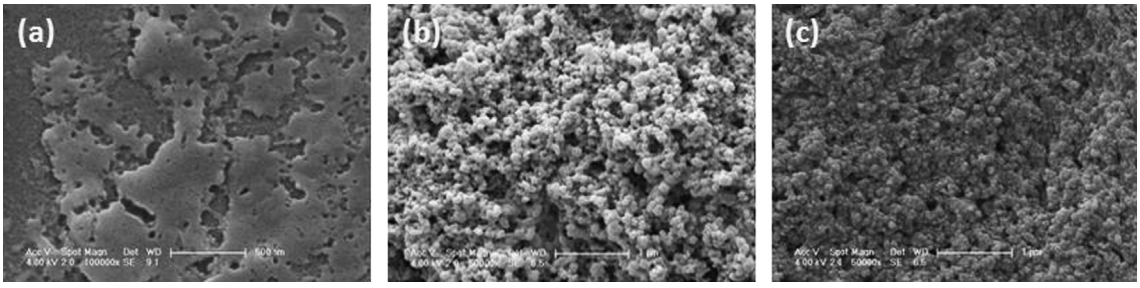

Fig. 3. SEM images of GFP fluorescent protein on (a) an ordinary microscope slide, (b) CdO, and (c) TiO_2 nanoparticles.

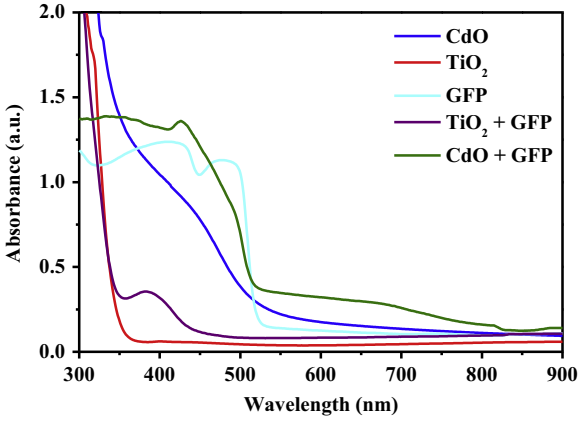

Fig. 4. Absorption spectra of metal oxide nanoparticles and GFP.

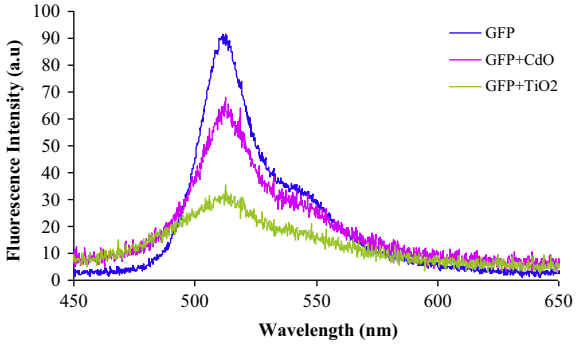

Fig. 5. Normalized fluorescence emission spectrum of GFP.

a nano-sphere, a nano-rod or a nano-particle [22–24]. Understanding and controlling the emission properties of molecules in nanostructured geometries has a great potential for applications in the area of nano-optics, biochemistry and molecular biology [25].

In our experiments, three different GFP solutions are prepared; such as GFP1 (dilute solution), GFP2 and GFP3 (concentrated solution) in order to control the concentration dependence of fluorescence lifetime of GFP molecule. While the intensity weighted fluorescence lifetime is measured as about 2.41 ns, the amplitude weighed fluorescence lifetime is measured as about 1.81 ns for all solutions (see Table 1). According to our experimental results, the fluorescence lifetime of GFP molecules are independent of fluorescent protein concentration.

In the second part of this work, the fluorescence lifetime of a free GFP molecule and a GFP molecule attached to a metal oxide nanoparticle (CdO and TiO_2) are compared. Decay parameters of GFP are analyzed using double-exponential fitting model and calculated lifetime values are summarized in Table 1. It is observed that the decay rates of the fluorescent molecules interacting with their surroundings are substantially different than those of free fluorescent molecules. When GFP molecules are embedded in CdO nanoparticles, the intensity weighted lifetime of the molecules is inhibited and its measured value is 1.881 ns. On the other hand, TiO_2 nanoparticles yield significantly more efficient inhibition of the decay parameters of GFP and the intensity weighted fluorescence lifetime of GFP decreases up to 1.375 ns.

The dynamics behind the quenching mechanism of GFP photoluminescence and the inhibition of the fluorescence lifetime of GFP is anticipated to be due to the energy transfer mechanism from GFP molecules to metal oxide nanoparticles. It is well know that an efficient energy transfer requires a good spectral overlap between GFP emission and nanoparticles absorption spectra. In our system, TiO_2 nanoparticles have an absorption capacity in the UV region as shown in Fig. 4. The spectral overlap region between the absorption spectrum of TiO_2 nanoparticles and the emission spectrum of GFP molecules is exactly zero; therefore, excitation energy of GFP cannot be transferred to TiO_2 nanoparticles. Moreover, the absorption spectrum of CdO nanoparticles has maximum intensity about 300 nm and the absorbance intensity becomes almost zero at 600 nm. The spectral overlapping area between the absorption spectrum of CdO nanoparticles and emission spectrum of GFP can be calculated using $J(\lambda)$ integral [26]. It is observed that there is a poor spectral overlap region but not enough to be a good FRET pair. Another important requirement of energy transfer is that donor and acceptor species are separated from each other in a nanometer scale. Energy can be transmitted over a very limited distance between 2 and 10 nm. GFP has a typical beta barrel structure with a diameter of about 24 Å and a height of 42 Å [3]. At the center of this barrel structure lies chromophore which is a short chain of altered amino-acids responsible for the light emission and the barrel structure is making GFP capable of fluorescing under almost any conditions. GFP molecules are chemically connected to metal oxide nanoparticles; therefore the distance between chromophore of GFP and nanoparticles is smaller than 2 nm. Thus, direct energy transfer between GFP and metal oxide

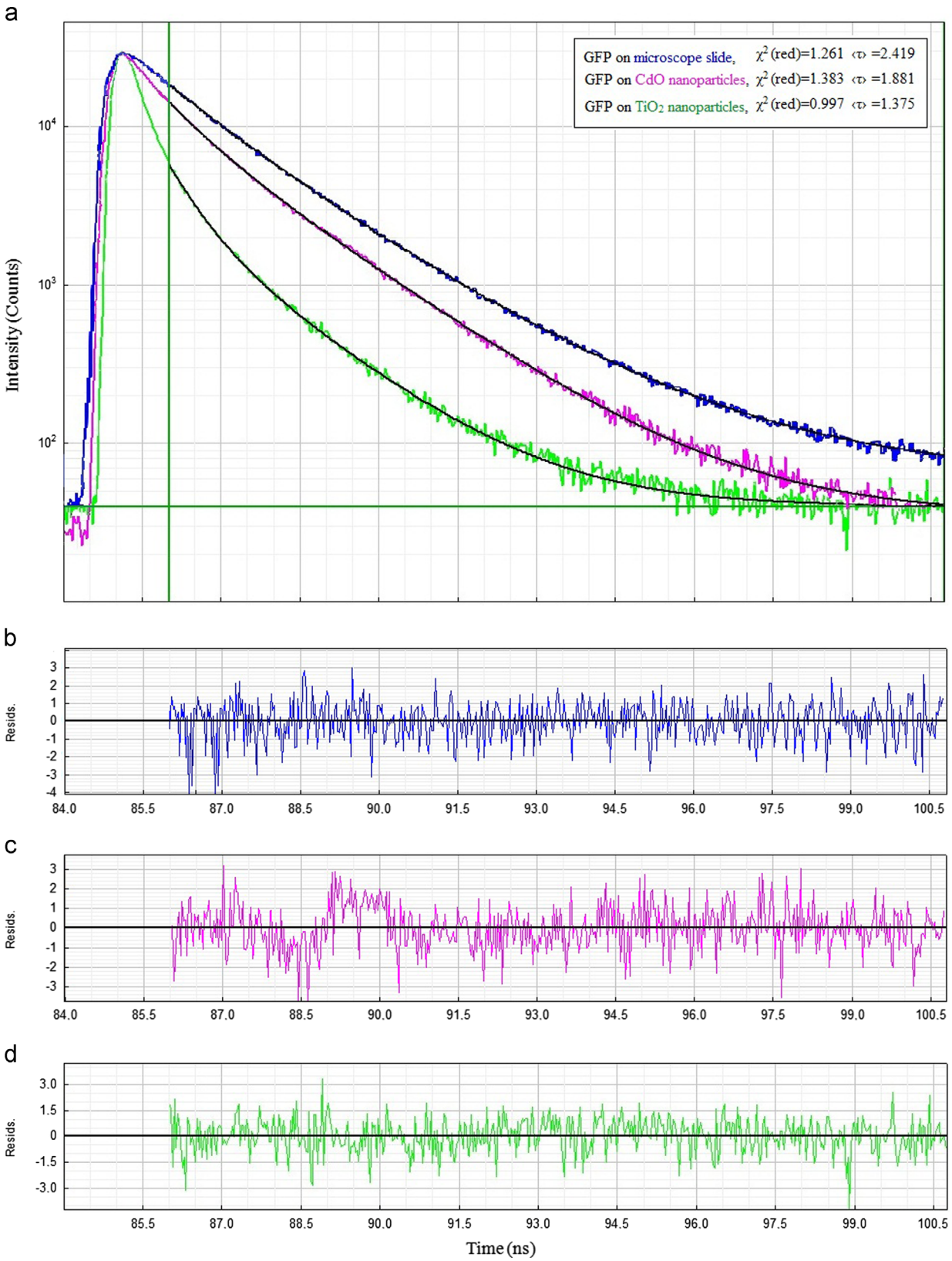

Fig. 6. (a) Fitting and calculation of decay parameters of GFP on (blue) microscope slide, (pink) CdO nanoparticles, (green) TiO_2 nanoparticles. (–) Indicates multi-exponential fitting curve. Residuals for fittings on (b) microscope slide, (c) CdO nanoparticles, and (d) TiO_2 nanoparticles. (For interpretation of the references to color in this figure legend, the reader is referred to the web version of this article.)

Table 1
Decay parameters for GFP.

Sample	A_1 (au)	τ_1 (ns)	A_2 (au)	τ_2 (ns)	$\langle\tau\rangle^a$ (ns)	$\bar{\tau}^b$ (ns)	χ^2
GFP1	13,881	3.006	18,239	0.903	2.411	1.812	1.416
GFP2	13,909	2.997	17,858	0.886	2.416	1.810	1.643
GFP3	11,020	2.942	12,735	0.847	2.419	1.818	1.261
GFP3+CdO	11,916	2.091	6090	0.782	1.881	1.648	1.383
GFP3+TiO_2	2323	1.732	3143	0.561	1.375	1.059	0.997

[a]The intensity weighted average lifetime (Eq. (3)).
[b]The amplitude weighted average lifetime (Eq. (4)).

nanoparticles, such as CdO and TiO_2, is also ruled out and the effective quenching mechanism is not caused by an energy transfer from GFP to MON.

Photoinduced electron transfer process is another important quenching mechanism that results in the decrease of the fluorescence lifetime of the GFP. Electron transfer kinetics can be evaluated in terms of Marcus theory [27,28]. The theory implies that the logarithm of the electron transfer rate is a quadratic function with respect to the driving force, $-\Delta G$. The simplified form of the rate constant of ET, k_{ET}, is given by

$$k_{ET} = A\exp\left[\frac{-(\Delta G^0+\lambda)^2}{4\lambda k_B T}\right] \quad (5)$$

where ΔG is the driving force, λ is the reorganization energy, k_B is Boltzmann's constant and T is the temperature. In the region of driving force smaller than the reorganization energy (the normal region), ET rate increases as driving force increases. This expression is successfully used by Kamat to investigate electron transfer kinetics between CdSe quantum dots and TiO_2 nanoparticles [29]. Electron transfer rate reaches a maximum value at $-\Delta G=\lambda$. When the driving force for reaction is greater than λ, inverted region kinetics are observed and ET rate increases as the driving force increases. Inverted region ET process is well established from experiments on systems with donor and acceptor distances fixed by protein framework [30].

The driving force for electron transfer between a photosensitizer and metal oxide nanoparticle can be dictated by the energy difference between the oxidation potential of photosensitizer and reduction potential of metal oxide nanoparticle. The Rehm–Weller equation can be utilized to determine the driving force energy changes for photoinduced electron transfer process [31]. This equation gives the driving force energy changes between a donor (D) and an acceptor (A) as

$$\Delta G^0 = e[E_{Oxi.}(D) - E_{Red.}(A)] - \Delta E^* \quad (6)$$

where e is the unit electrical charge, $E_{Oxi.}(D)$ and $E_{Red.}(A)$ are the oxidation and reduction potentials of electron donor and acceptor, respectively. ΔE^* is the electronic excitation energy corresponding to the energy gap between ground and the first excited states of donor species. In this study, GFP fluorescent protein is used as a photosensitizer and the excited state energy level of GFP depends on the photo physical formation of its chromophore. The chromophore of GFP, p-hydroxybenzylidene-imidazolinone (HBI), is formed by a cyclization reaction of three residues (Ser 65, Tyr 66 and Gly 67) in the main chain of GFP [32]. This chromophore is always located in the middle part of a central helix inside an eleven-stranded β-barrel and it plays an important role for the intense fluorescence of GFP [33]. Possible protonation states of the quantum mechanical chromophore model of GFP are neutral (HO_Y, N, O_X), anionic (O_Y, N, O_X), zwitterionic (O_Y^-, HN^+, O_X) and cationic (HO_Y, HN, O_X). In the study of photophyscis of GFP, it is determined that the neutral form of the chromophore absorbs light at 375 nm and the deprotonated anionic form absorbs at 494 nm. Excitation at both wavelengths leads to fluorescence emission at 509 nm. This is presumably due to the fact that the phenolic oxygen of Tyr 66 is more acidic in the excited state than in the ground state; excited-state proton transfer occurs resulting in a common anionic excited state that is responsible for the observed emission spectrum. Also, experimental estimate for the wavelength of absorption maximum in the cationic and zwitterionic form are 406 and 503 nm, respectively [34]. A computational analysis of the GFP chromophore and obtained absorption spectrum suggest that its chromophore has an anionic form. For computational analysis, ProtParam bioinformatics computer program is used. This program computes various physicochemical properties that can be deduced from a protein sequence. The computed parameters include the molecular weight, theoretical pI, amino acid composition, atomic composition, extinction coefficient, estimated half-life, instability index, aliphatic index and grand average of hydropathicity (GRAVY). The detailed results of ProtParam bioinformatics program are provided in the Supporting Information. Polyakov et al. described the ground and excited state electronic structures of anionic form of GFP chromophore and the S_{00} and S_{10} energy gap of anionic chromophore is computed as 2.37 eV. According to the absorption spectrum of our GFP chromophore, energy gap is calculated as 2.25 eV and this calculated result is in well agreement with Palyakov's results. Moreover, oxidation potential of the anionic form of GFP is determined as 0.47 V [35]. The energy level of conduction band edges for our TiO_2 nanoparticle which is known as a wide band gap semiconductor ($E_g=3.42$ eV) is calculated as -4.19 eV. On the other hand, a narrower band gap semiconductor CdO ($E_g=2.36$ eV) possesses a conduction band level around -4.45 eV. The electron transfer process from GFP to metal oxide nanoparticles and the band edge positions of metal oxides are shown in Fig. 7. Reduction potentials of metal oxides are given on the right according to the normal hydrogen electrode (NHE). The reduction potentials of CdO and TiO_2 are measured as -0.05 V and -0.31 V, respectively. Consequently, driving forces for CdO and TiO_2 are calculated as -1.73 eV and -1.47 eV using Eq. (6).

The reorganization energy (λ) of rigid dye molecules can be estimated from the stokes shift of the fluorescence spectrum [36]. According to the absorption and emission spectrum of green fluorescent protein, its reorganization energy should be ≤ 0.3 eV. This appears to be a typical value for rigid molecules, since calcultions by Moser et al. of solvent reorganization energy for coumarin-343, alizarin, and merocyanin Mc 2 in

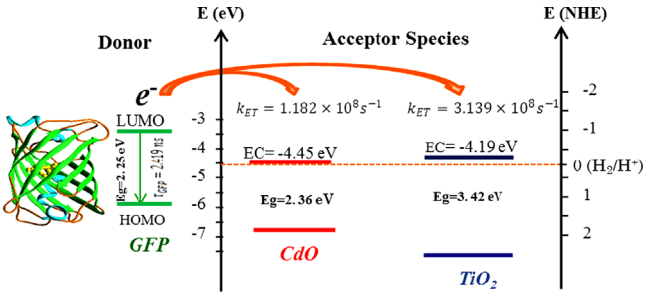

Fig. 7. Diagram of the electron transfer mechanism between GFP and metal oxide nanoparticles.

an ethanol–methanol mixture resulted in similar reorganization energies [37,38]. Because of the fact that reorganization energy of GFP is smaller than our calculated driving forces, the strong quenching of time resolved fluorescence lifetime under such conditions can be correlated to the inverted region photoinduced electron transfer process.

If we suppose that the observed decrease in fluorescence lifetime is entirely due to the photoinduced electron transfer process, the rate constant, k_{ET}, can be estimated by comparing the fluorescence lifetimes in the presence and absence of metal oxide nanoparticles (MON).

$$k_{ET} = \frac{1}{\tau_{GFP+MON}} - \frac{1}{\tau_{GFP}} \tag{7}$$

where τ_{GFP} and $\tau_{GFP+MON}$ are the fluorescence lifetimes of the GFP in the absence and presence of the metal oxide nanoparticles respectively. Using this relation, the electron transfer rate can be obtained from the fluorescence lifetime of GFP on CdO and TiO_2 metal oxide nanoparticles as shown in Table 2. The electron transfer rate, k_{ET}, of GFP on CdO and TiO_2 are 1.182×10^8 and $3.139 \times 10^8\ s^{-1}$, respectively. In fact, effective electron injection into the conduction band of the metal oxide nanoparticle is highly enhanced with the decrease of the energy difference between reduction of metal oxide nanoparticle and oxidation potential of GFP. This relation satisfies the inverted region electron transfer mechanism of Marcus model.

The time resolved fluorescence lifetime measurement of the emission of GFP reveal that electron transfer to the TiO_2 nanoparticles occurs with a characteristic time constant of 0.3 ns. However, more recent investigations with other sensitizing molecules show that the electron transfer occurs on a femtosecond time scale [36,39]. Since intraband and free electron transitions should be proportional to the density of states in the conduction band, the particle size is decisive in determining the photophysical and chemical properties of metal oxide nanoparticles [40]. In other words, the photoinduced electron transfer rate from a GFP molecule to a metal oxide nanoparticle can be controlled with the nanoparticle size. As the size of the semiconductor crystal changes, different facets and surface steps may be created. Small TiO_2 nanoparticles have a high surface area which gives rise to a lot of defects. Consequently, the surface defect density will be smaller for larger diameter (> 10 nm) systems, which makes the electron injection yield smaller. By decreasing the particle size of the metal oxides (TiO_2 and CdO), we can increase the electron transfer rate and obtain more efficient dye sensitized solar cells.

Table 2
Intensity weighted fluorescence lifetimes and electron transfer rate constants.

Sample	$\langle\tau\rangle^a$ *(ns)*	ΔG^0 *(eV)*	k_{ET} (s^{-1})
GFP3	2.419	–	–
GFP3+CdO	1.881	−1.73	1.182×10^8
GFP3+TiO_2	1.375	−1.47	3.139×10^8

4. Conclusion

The ensemble averaged electron injection dynamics from excited green fluorescent protein molecules to metal oxide nanoparticles is investigated by time-resolved fluorescence lifetime spectroscopy method. In our experimental studies of electron injection, TiO_2 and CdO nanoparticles are used as electron acceptors. Electron transfer process is monitored by the fluorescence emission spectrum intensity and fluorescence lifetime decay of GFP molecule. It is observed that fluorescence intensity of GFP is quenched due to electron transfer on the picosecond time scale. Furthermore, electron transfer process causes a significant decrease in the fluorescence lifetime of the GFP molecules. The rate of the electron transfer is calculated using fluorescence lifetime of GFP molecules. It is observed that employing a wide band gap metal oxide nanoparticle, such as TiO_2, give rises to more efficient photoinduced electron transfer process. The practical application of this system could be dye sensitized solar cell which has attracted wide attention for the potential application to convert sunlight into electricity. The energy conversion mechanism of dye-sensitized solar cells involves photoinduced electron transfer reactions. In this research, we have experienced the usefulness of green fluorescent molecule for dye sensitized solar cell device applications. We believe that the availability of efficient natural dye sensitizers such as fluorescent proteins may enhance the development of a long term stable dye sensitized solar cells.

Acknowledgments

This work was supported by TUBITAK (Contract numbers: 106T011 and 107T206), Bogazici University Research Fund (Contract numbers: 05HB301, 08HB301 and 13B03P4) and Karamanoğlu Mehmetbey University Research Fund (Contract number: 01-M-13).

Appendix A. Supplementary materials

Supplementary data associated with this article can be found in the online version at http://dx.doi.org/10.1016/j.ceramint.2013.10.017.

References

[1] S. Brasselet, E.J.G. Peterman, A. Miyawaki, W.E. Moerner, Single-molecule fluorescence resonant energy transfer in calcium-concentration-dependent cameleon, J. Phys. Chem. B 104 (2000) 3676–3682.

[2] A. Furtado, R. Henry, Measurement of green fluorescent protein concentration in single cells by image analysis, Anal. Biochem. 310 (2002) 84–92.

[3] M. Zimmer, Green fluorescent protein (GFP): applications, structure, and related photophysical behavior, Chem. Rev. 102 (2002) 759–781.

[4] R. Tsien, The green fluorescent protein, Annu. Rev. Biochem. 67 (1998) 509–544.

[5] J. Wiedenmann, F. Oswald, G.U. Nienhaus, Fluorescent proteins for live cell imaging: opportunities, limitations, and challenges, IUBMB Life 61 (2009) 1029–1042.

[6] M. Chalfie, Y. Tu, G. Euskirchen, W.W. Ward, D.C. Prasher, Green fluorescent protein as a marker for gene expression, Science 263 (1994) 802–805.

[7] M. Elangovan, R.N. Day, A. Periasamy, Nanosecond fluorescence resonance energy transfer-fluorescence lifetime imaging microscopy to localize the protein interactions in a single living cell, J. Microsc. 205 (2002) 3–14.

[8] A.M. Bogdanov, A.S. Mishin, I.V. Yampolsky, V.V. Belousov, D.M. Chudakov, F.V. Subach, V.V. Verkhusha, S. Lukyanov, K.A. Lukyanov, Green fluorescent proteins are light-induced electron donors, Nat. Chem. Biol. 5 (7) (2009) 459–461.

[9] G. Bisker, M. Limor, D. Yelin, Controlled fabrication of gold nanoparticle and fluorescent protein conjugates, Plasmonics 7 (4) (2012) 609–617.

[10] Y. Fu, J. Zhang, J.R. Lakowicz, Metal-enhanced fluorescence of single green fluorescent protein (GFP), Biochem. Biophys. Res. Commun 376 (2008) 712–717.

[11] P.V. Kamat, Photochemistry on nonreactive and reactive (semiconductor) surfaces, Chem. Rev. 93 (1) (1993) 267–300.

[12] J. Livage, M. Henry, C. Sanchez, Sol–gel chemistry of transition metal oxides, Prog. Solid State Chem. 18 (1988) 259–341.

[13] M.R. Hoffmann, S.T. Martin, W. Choi, D.W. Bahnemann, Environmental applications of semiconductor photocatalysis, Chem. Rev. 95 (1995) 69–96.

[14] G. Oskam, Z.S. Hu, R.L. Penn, N. Pesika, P.C. Searson, Coarsening of metal oxide nanoparticles, Phys. Rev. E 66 (2002) 011403-1–011403-4.

[15] S.J. Pearton, D.P. Norton, K. Ip, Y.W. Heo, T. Steiner, Recent progress in processing and properties of ZnO, Prog. Mater. Sci. 50 (2005) 293–340.

[16] J.M. Rehm, G.L. McLendon, Y. Nagasawa, K. Yoshikara, J. Moser, M. Gratzel, Femtosecond electron-transfer dynamics at a sensitizing dye–semiconductor (TiO_2) interface, J. Phys. Chem. 100 (1996) 9577–9578.

[17] H.M. Cheng, W.F. Hsieh, Electron transfer properties of organic dye-sensitized solar cells based on indoline sensitizers with ZnO nanoparticles, Nanotechnology 21 (2010) 485202–485209.

[18] J. Millan, Wide band-gap power semiconductor devices, IET Circuits Devices Syst. 1 (5) (2007) 372–379.

[19] H.N. Ghosh, Effect of strong coupling on interfacial electron transfer dynamics in dye-sensitized TiO_2 semiconductor nanoparticles, J. Chem. Sci. 119 (2) (2007) 205–215.

[20] S. Acikgoz, I. Sarpkaya, P. Milas, M.N. Inci, G. Demirci, R. Sanyal, Investigation of fluorescence dynamics of BODIPY embedded in porous silicon and monitoring formation of a SiO_2 layer via a confocal FLIM-based NSET method, J. Phys. Chem. C 115 (2011) 22186–22190.

[21] J. Tauc, R. Grigorovici, A. Vancu, Optical properties and electronic structure of amorphous germanium, Phys. Status Solidi B 15 (1966) 627–637.

[22] S. Astilean, S. Garrett, P. Andrew, W.L. Barnes, Controlling the fluorescence lifetime of dyes in nanostructured geometries, J. Mol. Struct. 651 (2003) 277–283.

[23] R. Bardhan, N.K. Grady, J.R. Cole, A. Joshi, N. Halas, Fluorescence enhancement by Au nanostructures: nanoshells and nanorods, J. ACS Nano 3 (2009) 744–752.

[24] M.R. Vasic, L.D. Cola, H. Zuilhof, Efficient energy transfer between silicon nanoparticles and a Ru−polypyridine complex, J. Phys. Chem. C 113 (2009) 2235–2240.

[25] E.C. Wu, J.H. Park, J. Park, E. Segal, F. Cunin, M.J. Sailor, Oxidation-triggered release of fluorescent molecules or drugs from mesoporous Si microparticles, ACS Nano 2 (2008) 2401–2409.

[26] S. Acikgoz, G. Aktas, M.N. Inci, H. Altin, A. Sanyal, FRET between BODIPY azide dye clusters within PEG-based hydrogel: a handle to measure stimuli responsiveness, J. Phys. Chem. B 114 (34) (2010) 10954–10960.

[27] R.A. Marcus, N. Sutin, Electron transfers in chemistry and biology, Biochim. Biophys. Acta 811 (1985) 265–322.

[28] R.A. Marcus, On the theory of electron-transfer reactions. VI. Unified treatment for homogeneous and electrode reactions, J. Chem. Phys. 43 (1965) 679–701.

[29] P.V. Kamat, Quantum dot solar cells. Semiconductor nanocrystals as light harvestors, J. Phys. Chem. C 112 (2008) 18737–18753.

[30] P.L. Dutton, C.C. Mosser, Quantum biomechanics of long-range electron transfer in protein: hydrogen bonds and reorganization energies, Proc. Natl. Acad. Sci. USA 91 (1994) 10247–10250.

[31] D. Rehm, A. Weller, Kinetics of fluorescence quenching by electron and H-atom transfer, Isr. J. Chem. 8 (1970) 259–271.

[32] O. Shimomura, Structure of the chromophore of Aequorea green fluorescent protein, FEBS Lett. 104 (1979) 220–222.

[33] F. Yang, L.G. Moss, G.N. Phillips, The molecular structure of green fluorescent protein, Nat. Biotechnol. 14 (10) (1996) 1246–1251.

[34] I.V. Polyakov, B.L. Grigorenko, E.M. Epifanovsky, A.I. Krylov, A.V. Nemukhin, Potential energy landscape of the electronic states of the GFP chromophore in different protonation forms: electronic transition energies and conical ıntersections, J. Chem. Theory Comput. 6 (2010) 2377–2387.

[35] K.B. Bravaya, M.G. Khrenova, B.L. Grigorenko, A.V. Nemukhin, A.I. Krylov, Effect of protein environment on electronically excited and ionized states of the green fluorescent protein chromophore, J. Phys. Chem. B 115 (2011) 8296–8303.

[36] M. Hilgendorff, V. Sundstrom, Dynamics of electron ınjection and recombination of dye-sensitized TiO_2 particles, J. Phys. Chem. B 102 (1998) 10505–10514.

[37] J.E. Moser, M. Gratzel, Photosensitized electron injection in colloidal semiconductors, J. Am. Chem. Soc. 106 (1984) 6557–6564.

[38] J.E. Moser, M. Gratzel, D.K. Sharma, N. Serpone, Picosecond time-resolved studies of photosensitized electron injection in colloidal semiconductors, Helv. Chim. Acta 68 (1985) 1686–1690.

[39] Y. Tachibana, J.E. Moser, M. Gratzel, D.R. Klug, J.R. Durrant, Subpicosecond interfacial charge separation in dye-sensitized nanocrystalline titanium dioxide films, J. Phys. Chem. 100 (1996) 20056–20062.

[40] L. Du, A. Furube, K. Hara, R. Katoh, M. Tachiya, Mechanism of particle size effect on electron ınjection efficiency in ruthenium dye-sensitized TiO_2 nanoparticle films, J. Phys. Chem. C 114 (18) (2010) 8135–8143.